Mine Water and the Environment (2023) 42:134–145
https://doi.org/10.1007/s10230-022-00911-5

TECHNICAL ARTICLE

Fuzzy Risk Assessment of a Stormwater Storage System in a Poorly Gauged Mine Site: The Case of the Golgohar Mine Site

Siamak Rezazadeh Baghal[1] · **Saeed Reza Khodashenas**[1]

Received: 1 February 2022 / Accepted: 6 December 2022 / Published online: 19 December 2022

Abstract

Although many approaches have been proposed for flood risk assessment in urban areas, an equivalent methodology for remote mine sites with poor hydrological data records is still needed. This paper provides a fuzzy methodology based on calculating the hydrological return period discharge and the resistance-load theory for embankment failure risk assessment of an existing drainage storage system (lake) at the Golgohar mine site. The uncertainty of the two uncertain components, load and resistance, were endowed with triangular fuzzy numbers (TFNs) describing possible values the two components may have. First, based on a comparison of two consecutive Sentinel-2A images and the model water volume, a new manual storm water management model (SWMM) calibration technique was introduced. Then, three well-known synthetic rainfall hyetograph generation methods based on a single point of the rainfall curve were input into the calibrated SWMM model. Second, the BRCH-J model was used to calculate the maximum water level in the lake if an embankment breach occurs in two scenarios, with an unprotected and a fully riprap-protected downstream face. Afterward, the SWMM and BRCH-J outputs were used to define the TFN parameters representing the load (surface flow) and resistance (lake capacity). Finally, on the basis that both TFNs must match, a fuzzy risk product with alpha-cut principles was defined, as was the difference between the TFNs representing the load and resistance. The result indicates that the available stormwater storage volume exceeded the expected capacity; the risk of embankment failure was 0.15%, which was less than the design risk (1%, based on the hydrological return period concept).

Keywords Embankment failure · Sentinel-2A image · SWMM calibration · Remote area · Fuzzy number

Introduction

Mining and agriculture are considered the primary industries of human civilization (Hartman and Mutmansky 2002). Nonetheless, mining harms the environment and can destroy an area much larger than the mine site itself (Worldwide 2010). Besides, mining developments invariably have significant interaction with the local drainage system, which make many mining operations prone to flooding. As a result, workers' lives are more threatened by environmental hazards. This situation is exacerbated by the lack of a formal engineering criteria. For instance, it is necessary for companies worldwide to rehabilitate mine sites to a safe state. However, there is a lack of guidance for defining achievable and measurable criteria that reflect rehabilitation success (Manero et al. 2020). In addition, because of mining activities, natural drainage systems are relocated into a new artificial channel. Unfortunately, available mine operations criteria do not sufficiently consider current drainage system diversion practice due to the absence of guidelines for implementing post-mining diversion channels (Flatley and Markham 2021). Across the globe, a total of 6000 active mining sites have been reported (Maus et al. 2020). However, there has been no exhaustive analysis of the flood risk in the mining sites. Since the Golgohar mine site is located in a dry region with inadequate streamflow data, it is susceptible to inaccurate flood risk estimation that may threaten many workers' lives.

Probability theories and fuzzy methods have been widely used for risk assessment for drainage storm design in catchment scales (Caradot et al. 2011; Cheng et al. 2017; Fu et al. 2013; Lee and Kim 2019; Rezazadeh Baghal and Khodashenas 2022a, b; Sun et al. 2012; Ursino 2015). However, due to

✉ Saeed Reza Khodashenas
khodashenas@ferdowsi.um.ac.ir

Siamak Rezazadeh Baghal
siamak.rezazadehbaghal@mail.um.ac.ir

[1] Water Engineering Department, Ferdowsi University of Mashhad, Mashhad, Iran

a lack of historical data, probabilistic methods are not preferred (Salah and Moselhi 2015). It is, for instance, reported by the International Organization for Standardization (ISO 2009) that the risk of flooding is unclear, mainly due to a lack of historical data. Zadeh (1973) first introduced fuzzy logic to deal with problems in the probabilistic methods that handle approximate reasoning. Afterward, Shrestha et al. (1990) introduced the fuzzy risk concept, defined as the difference between the fuzzy numbers representing the resistance and the load in a system, to overcome the limitation of probabilistic methods in engineering practice. Since then, fuzzy risk techniques have been used in many civil and environmental engineering projects. For instance, Su and Wen (2013) assumed resistance force and load acting on a gravity dam as uncertain parameters to conduct a fuzzy number risk model for a dam instability risk assessment. Rezazadeh Baghal and Khodashenas (2022a, b) used the fuzzy risk concept for an optimal design of a rectangular canal, where canal capacity and runoff are uncertain parameters. For the fuzzy risk assessment of an existing drainage storage system at the Golgohar mine site, TFNs were used to represent the uncertainty related to lake capacity (resistance) and surface runoff (load). Overall, the two uncertain components in this study were obtained from a calibrated storm water management model (SWMM) and a breach erosion model (BRCH-J).

Among hydrological models, SWMM is widely used for calculating and analyzing the hydrologic characteristic of an area (Rossman 2010). SWMMs must be calibrated and validated before they are used for stormwater management. For SWMM calibration techniques, manual (Shamsi and Koran 2017) and automatic calibration (Behrouz et al. 2020; Dent et al. 2004; Mancipe-Munoz et al. 2014) techniques have been discussed in the literature. For instance, Barco et al. (2008) used 10 storm events for SWMM calibration and validation in a large urban catchment. Sangal and Bonema (1994) developed and applied a method for SWMM calibration for many urban catchments in the United States beyond the measured data (runoff values) to verify the model parameters. This paper presents a novel SWMM calibration technique based on a series of Sentinel-2A images. The definition parameters of the TFN representing the surface runoff were obtained based on the limit interval and the mean value of the calibrated SWMM outputs.

BRCH-J was first developed by the National Weather Service (NWS) and coded in FORTRAN. BRCH-J can predict the breach parameters (the size and shape of the embankment breach opening and time of formation) and the outflow hydrograph of an earthen flood embankment (Singh 1996). This model was chosen because of its capability to perform breach simulations that consider the rip-rap size in the downstream face of the embankment. The definition parameters of the TFN representing the lake capacity (resistance) in our experimental catchment were obtained from the results of an embankment breach simulation model.

In light of the above methods, this study provides a state-of-the-art fuzzy risk methodology for reexamining the risk of an embankment failure within a lake stormwater storage system in the Golgohar mine site, incorporating the load and resistance theory. Since the return period and risk of failure are related quantities (Salas et al. 2013), we used the fuzzy method for the first time to study risk based on the hydrological return period. Moreover, Sentinel-2A images were used to calibrate the SWMM model, which is absent in previous studies. Using Sentinel-2A images is beneficial for a remote mine site, providing many high-resolution (10 m) images with a short revisit time (about 10 days). In addition, the proposed approaches to obtain the TFNs representing the runoff volume and the lake capacity are unique. The fuzzy membership functions were applied to hydraulic and hydrologic uncertain components, indicating another gap in the current literature. Later, the proposed fuzzy methodology was applied to a mine site in Iran, aiming TFNs representing the load and resistance. The presented method is advantageous when the historical data is scarce and enables decision-makers to be more prepared when taking actions to combat the consequences of flooding in a remote mine site. This paper is structured as described in Fig. 1.

Overview of the Study Area

The Golgohar iron ore mine site (open-pit mine) is located in Sirjan county (LAT: 29.10121 and LAN: 55.32306 decimal degrees), in Kerman province, Iran. The land use in the Golgohar mine site and the lake location are shown in Fig. 2. The Golgohar dewaters (4000–5000 m^3/day) its large open pits to prevent flooding (Jahanshahi and Zare 2017). The Golgohar mine site has a basin area of 27.2 km^2, as depicted in Fig. 3. The mainland cover is bare soil (72%) andthe most of the rest is industrial areas. Based on the Köppen climate classification scheme, our study area has a BSk (cold semi-arid) climate. The mean annual precipitation is around 150 mm yr^{-1} and potential evaporation of ≈ 3000 mm yr^{-1}. Rainfall occurs only in specific months and most of the rain is centered in April, with an average total accumulation of 100 mm. The rain gauge station is placed inside the mine site, and there is no hydrometric station to measure runoff in our study area. The drainage system of the mine site consists of two main storm drain canals (total length = ≈ 6.5 km) and a storage drainage system (maximum area and volume capacity are 17.26 ha and 0.167 Mcm, respectively) that receives runoff via only surface flow. The lake storage capacity is enhanced with a relatively long homogeneous embankment without any spillway to release excess water. For the risk assessment of the embankment failure, our study

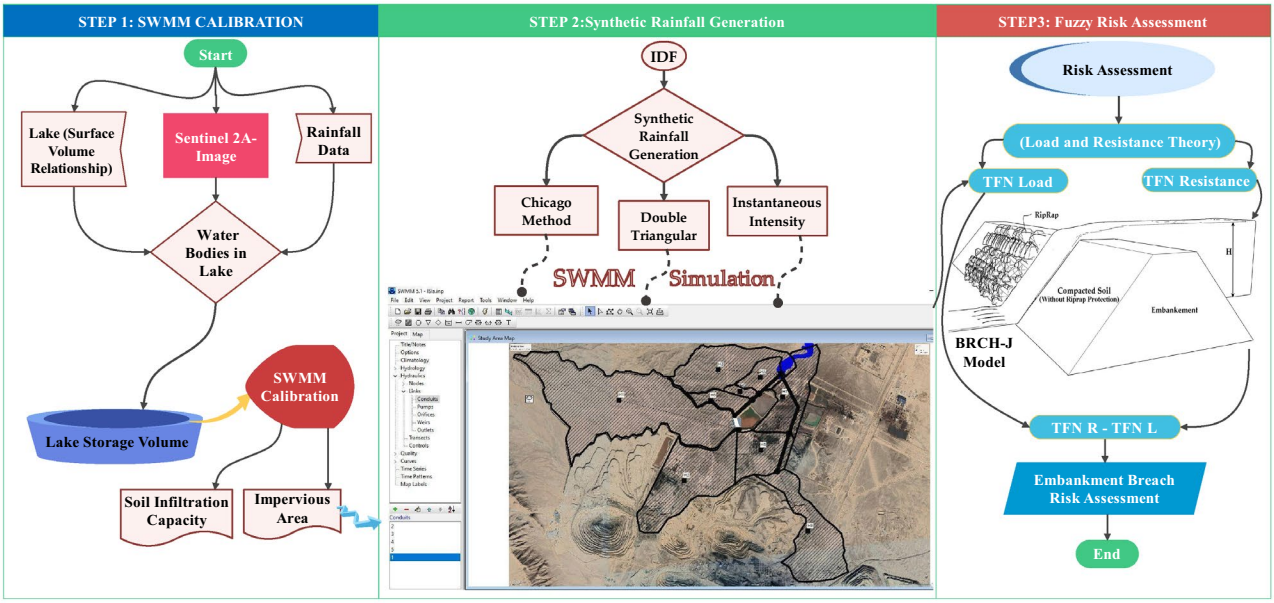

Fig. 1 Flow chart of this study

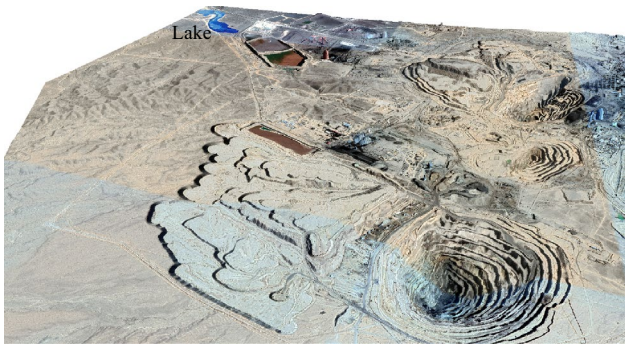

Fig. 2 The land use in the GolGohar mine site and the location of the lake storage system (Map © 2022 Google, Image © 2022 Maxar Technologies, Image.© 2022 CNES/Airbus)

area is divided into nine sub-catchments (Fig. 3). It is worth mentioning that the Golgohar mining sector meets 30% of steel factory needs in Iran (Shahba et al. 2017).

The Fuzzy Risk Concepts

Triangular Fuzzy Number

The triangular fuzzy number consists of three parameters (a, b, c), where a and c represent the smallest and largest likely value, respectively, and b is the most probable value. The TFN membership function (μ_A)is given by (Chaira 2019):

$$\mu_A(x) = \begin{cases} 0, x < a, x > c \\ \dfrac{x - a}{b - a}, a \le x \le b \\ \dfrac{c - x}{c - b}, b < x \le c \end{cases} \quad (1)$$

Fuzzy Risk with the Alpha-cut Principle

In the task of stormwater storage risk assessment, the system has a load L (surface runoff) and a resistance R (lake storge), both represented by fuzzy numbers. Taking the alpha-level of intervals of L and R, the fuzzy number of the safety margin can be calculated as below (Shrestha et al. 1990);

$$Z^{\alpha} = R^{\alpha} - L^{\alpha}, \alpha \in [0, 1] \quad (2)$$

Triangular fuzzy products representing the load (surface runoff) $R = [R_1, R_2, R_3]$ and the resistance (lake capacity) $L = [L_1, L_2, L_3]$ with alpha-cut principle are obtained as below:

$$R^{\alpha} = [r_1^{\alpha}, r_2^{\alpha}] = [R_1 + \alpha(R_2 - R_1), R_3 - \alpha(R_3 - R_2)],$$
$$and\ L^{\alpha} = [l_1^{\alpha}, l_2^{\alpha}] = [L_1 + \alpha(L_2 - L_1), L_3 - \alpha(L_3 - L_2)] \quad (3)$$

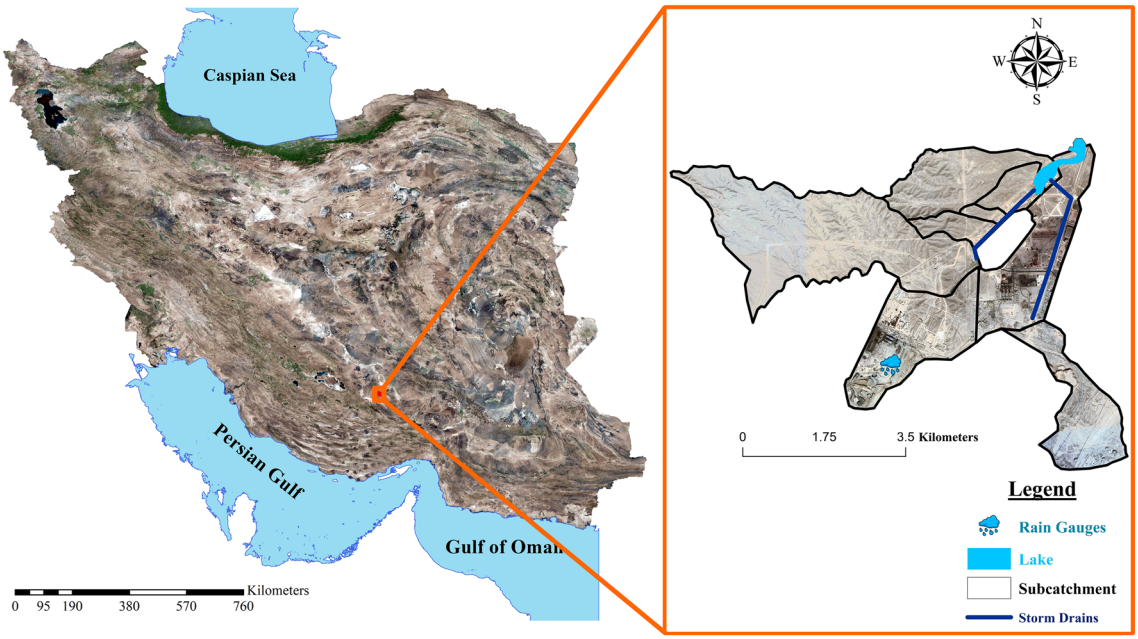

Fig. 3 The location map of the GolGohar mine site (Map © 2022 Google, Image © 2022 Maxar Technologies, Image. © 2022 CNES/Airbus)

The fuzzy risk may be defined as the area of fuzzy safety margin where values of Z are negative. The fuzzy risk product is obtained as;

$$\begin{aligned} Z^{\alpha} &= [R-L]^{\alpha} = \left[R_1+\alpha\left(R_2-R_1\right),\ R_3-\alpha\left(R_3-R_2\right)\right] \\ &\quad -\left[L_1+\alpha\left(L_2-L_1\right),\ L_3-\alpha\left(L_3-L_2\right)\right] \\ &= [R_1+\alpha\left(R_2-R_1+L_3-L_2\right) \\ &\quad -L_3\ ,\ R_3-\alpha\left(R_3-R_2+L_2-L_1\right)-L_1] \end{aligned} \tag{4}$$

$$\begin{aligned} &\text{Since } \alpha \in [0,1],\ \text{so at } \alpha = 0,\ [\mathrm{R}-\mathrm{L}]^0 \\ &= [\mathrm{R}_1 - \mathrm{L}_3, \mathrm{R}_3 - \mathrm{L}_1] \text{ and at } \alpha = 1,\ [\mathrm{R}-\mathrm{L}]^1 = [\mathrm{R}_2 - \mathrm{L}_2] \end{aligned} \tag{5}$$

$$\text{Thus, } \mathrm{R}-\mathrm{L} = [\mathrm{R}_1 - \mathrm{L}_3, \mathrm{R}_2 - \mathrm{L}_2, \mathrm{R}_3 - \mathrm{L}_1]. \tag{6}$$

$$\begin{aligned} &\text{Let, } \mathrm{R}_1+\alpha\left(\mathrm{R}_2-\mathrm{R}_1+\mathrm{L}_3-\mathrm{L}_2\right)-\mathrm{L}_3=0,\ \text{and} \\ &\mathrm{R}_3-\alpha\left(\mathrm{R}_3-\mathrm{R}_2+\mathrm{L}_2-\mathrm{L}_1\right)-\mathrm{L}_1=0 \end{aligned} \tag{7}$$

Then, we have, $\alpha = \frac{L_3-R_1}{R_2-R_1+L_3-L_2}$ and $\alpha = \frac{R_3-L_1}{R_3-R_2+L_2-L_1}$, so, based on Eq. 5, the fuzzy risk values when $R_2 \geq L_2$, $R_2 \leq L_2$, are obtained as:

$$\text{Risk} = \begin{cases} \dfrac{\frac{(R_1-L_3)^2}{R_2-R_1+(L_3-L_2)}}{R_3-L_1-(R_1-L_3)}, \text{ for } R_2 \geq L_2 \\ 1-\dfrac{\frac{(R_3-L_1)^2}{R_3-R_2+L_2-L_1}}{R_3-L_1-(R_1-L_3)}, \text{ for } R_2 \leq L_2 \end{cases} \tag{8}$$

The definition parameters of TFNs representing the surface runoff and lake capacity are obtained from the outputs of the calibrated SWMM and the BRCH-J models, as discussed in the following sections.

The SWMM Calibration Process

Since only the stormwater conversion into a surface runoff volume is needed to be addressed, the SWMM is tuned by adjusting only impervious areas and the SCS curve number in the catchment. So, manual trial and error with the subjective procedure (expert judgment) are utilized here for calibrating SWMM. Hence, if the model (SWMM output) water volume is less than the observed value (based on comparing two consecutive Sentinel-2A images), the SCS curve number should be increased.

Sentinel-2A Images

Since Sentinel-2A's revisit time is around 10 days, comparing the water bodies extracted from two consecutive Sentinel-2A images immediately before and after a rainfall event provides the amount of runoff volume stored in the lake at the mine site after the rainfall occurs. The lake surface-volume relationship was obtained using a high-resolution digital elevation model (DEM). The task of the SWMM manual trial and error calibration technique is to calculate the modeled runoff volume that approximates the one obtained from

comparing two consecutive Sentinel-2A images. Overall, for the manual SWMM calibration, 20 Sentinel-2A images were collected from before and after 10 rainfall events over seven years (2015–2022). Since our study area was relatively small, the rainfall pattern was assumed to be the same in the entire catchment. Due to the short time between two consecutive Sentinel-2A images (Fig. 4a, b), evaporation from the lake was considered negligible.

To extract water bodies from Sentinel-2A images, the modified normalized difference water index (MNDWI) equation and a band sharpening algorithm were utilized (Yang et al. 2017). The MNDWI equation with the spatial resolution of 10 m is:

$$\mathrm{MNDWI}_{10\mathrm{m}} = \frac{\rho_3 - \rho_{11}^{10\mathrm{m}}}{\rho 3 + \rho_{11}^{10\mathrm{m}}} \tag{9}$$

where ρ_3 is the green band and $\rho_{11}^{10\mathrm{m}}$ is the downscaling of band 11 of the Sentinel-2A image. Since the Golgohar mine site is located in a dry region, typically rainfall events occur after a prolonged dry period. Rain gauge data has proven this. Therefore, the initial moisture that affects the initial infiltration and total infiltration capacity was considered the same for all rainfall scenarios. For storm-by-storm SWMM calibration, the two following sequences were performed.

SWMM Calibration Model Water Volume for the Percentage of Impervious Area and its Depth of Depression Storage

Two parameters that need to be calibrated here are the percentage of impervious area and the depth of depression storage of this impervious area. However, to decrease the total time of the calibration process, the initial guess for the impervious area percentage was first derived from the Sentinel-2A images. So, the normalized difference vegetation index (NDVI) is used, in which the impervious area has an NDVI value > zero. The NVDI is obtained as below (Zha et al. 2003);

$$\mathrm{NDVI} = \frac{\rho_{\mathrm{SWIR1}} - \rho_{\mathrm{NIR}}}{\rho_{\mathrm{SWIR1}} + \rho_{\mathrm{NIR}}} \tag{10}$$

where ρ_{SWIR1} and ρ_{NIR} are the reflectance of band 11 and band 8 of the Sentinel-2A image. The obtained initial value for the impervious area percentage will be used for the rest of the manual SWMM calibration processes that follow.

The proper calibration process for determining the percentage of impervious areas is to consider only low-intensity rainfall scenarios in which their intensities are less than the infiltration capacity of the previous land (Sangal and Bonema 1994). Hence, only impervious areas contributed to runoff production. In the following, the modeled runoff volume resulting from the impervious areas is compared with the observed volume (Eq. 9) after adjusting the depth of depression storage on impervious areas. As a result, if the modeled water volume exceeds the observed one, the depth of the depression storage is increased. The converse holds when the observed water volume exceeds the SWMM results. This process continues until a good match is obtained between the percentage of impervious areas and the depth of depression storage. Their final values are recorded for each storm event.

SWMM Model Calibration for SCS Curve Number and Depth of Depression Storage

The two parameters that need to be addressed in this section are the SCS curve number and the initial abstraction of the pervious area. To do so, high-intensity rainfalls in which intensities are more than the soil infiltration capacity of the basin are selected. Hence, if the model water volume is more than

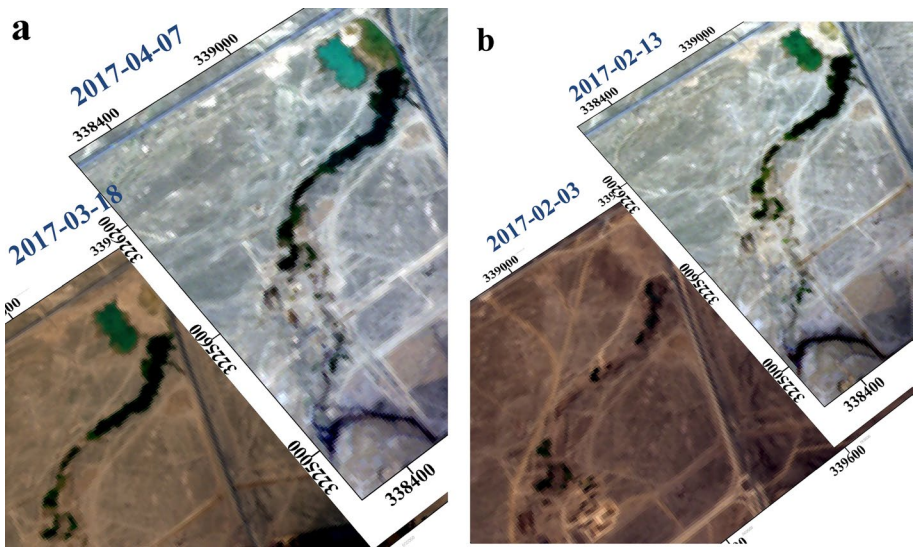

Fig. 4 Two consecutive Sentinel-2A images before and after a rainfall event **a** after 68.5 mm rainfall event **b** after 128.5 mm rainfall event

the observed volume, the SCS curve number is decreased. The converse holds when the model output estimates less runoff volume. (Sangal and Bonema 1994). This process continues until an appropriate match is obtained between the SCS curve number and the initial abstraction of the pervious area. Similarly, their final values are recorded for each storm event.

Synthetic Rainfall Generation Technique

Three well-known methods for generating synthetic hyetographs, named Chicago, doubled triangular, and instantaneous intensity (Chow et al. 1988) methods, were considered to act as inputs of the calibrated SWMM. Their basic prerequisite parameters were obtained directly from the single point of the intensity duration frequency (IDF) curve for a particular frequency. The IDF can be described by:

$$i = \frac{a}{(t_d + c)^b} \tag{11}$$

where: i = the maximum intensity (mm/h) corresponding to a rainfall duration t_d (min); and a, b, and c = coefficients that vary with the location and return period. In our experimental catchment, the resulting values for these parameters were a = 84.239, b = 0.441, and c = 0 for the 100-year return period. As a result, the total rainfall depth for a 50-h duration was calculated as 124.3 mm. The choice of T = 100-year return period, as well as a 50-h storm event, was part of the initial design requirements, in which the lake system was designed with a week of emptying time for a 50-h storm event.

Chicago Method

KEIFER and Chu (1957) first introduced the Chicago design synthetic hyetograph method to define the design rainfall in urban areas as below;

$$i(t) = \frac{a\left[\frac{t}{n}(1-b)+c\right]}{\left[\frac{t}{n}+c\right]^{1+b}} \tag{12}$$

where; $n = \frac{t_p}{t_d}$ for $t \le t_p$ and $n = 1 - \frac{t_p}{t_d}$ for $t > t_p$, and t_p is the time antecedent to the peak intensity.

Double Triangular Method

LEE and Ho (2008) first introduced the double triangle method to account for typhoon rainstorms, which is derived from a single point of the IDF curves. For a 50 h and 124.3 mm depth rainfall scenario, we have;

$$i(t) = \begin{cases} (124.3 - d_m)\dfrac{t}{t_1 t_2}; 0 \le t \le t_2 \\ 4d_m \dfrac{t - t_1}{(50 - 2t_1)^2}; t_2 \le t \le 25 \\ 4dm \dfrac{50 - t_1 - t}{(50 - 2t_1)^2}; 25 \le t < 50 - t_2 \\ (124.3 - d_m)\dfrac{50 - t}{t_1 t_2}; 50 - t_2 \le t \le 50 \end{cases} \tag{13}$$

where: $t_1 = \frac{1}{2}(50 - t_m)$, $t_2 = t_1 + (124.3 - d_m)\frac{t_m^2}{4t_1 d_m}$ i(t) = rainfall intensity at time t, d_m = rainfall depth corresponding to duration t_m, which is obtained from the IDF curve, and t_m = duration of the central triangular hyetograph. For $t_m = 0$ and $t_m = t_d$ (rainfall duration), the double triangular turns to single triangular hyetograph.

Instantaneous Intensity Method

The principle behind this method was first introduced by Chow et al. (1988). The times of intersection before and after peak are labeled, t_a, and t_b, respectively, and the total time between intersections is obtained by $T_d = t_a + t_b$. The total amount of rainfall (R) is then given by;

$$R = T_d . i_{ave} \tag{14}$$

where $T_d = \frac{t_a}{r} = \frac{t_b}{1-r}$ and r is the storm advancement coefficient (uncertain parameter). Following Chow et al. (1988), Eq. 14 is differentiated with respect to T_d. Knowing that:

$$i_{avg} = \frac{a}{(T_d + c)^b}, \tag{15}$$

the instantaneous intensity is obtained by:

$$i = \frac{dR}{dT_d} = \frac{a[(T_d + c)^b - bT_d(T_d + c)^{b-1}]}{(T_d + c)^{2b}} \tag{16}$$

Breach Modeling

In our experimental catchment, the capacity of the existing lake stormwater storage system was increased by a 510 m long homogeneous embankment of compacted soil (Fig. 5). This earth-fill embankment, 5 m high and 3 m wide at its crest, has 0.167 Mcm capacity at its crest level. Its upstream and downstream slope was constructed at 1.65 H: IV and 2.1 H: 1 V, and it is poorly rip-rap protected. The predominant mechanism of breaching is the erosion of the material by the flow of water over the crest. Due to local weaknesses (poor compaction, poor material, and poor design), erosion may be initiated at any location where local shear exceeds a critical

Fig. 5 The stormwater storage system (lake with an earth-fill embankment) in the GolGohar mine site. (Map © 2022 Google, Image. © 2022 CNES/Airbus)

value, after which the soil particles are set in motion (Singh 1996). Hence, an embankment breach due to overtopping can occur at any water level above the crest level.

The BRCH-J model was used here for the breach simulation due to overtopping. Since the erosive capacity of the flowing waters for riprap-protected faces is less than for unprotected ones, two scenarios were defined here for breach modeling. The maximum water levels above the existing embankment crest and its associated volumes once the breach occurs in each scenario—unprotected and fully riprap protected embankments—are depicted in Fig. 6a, b. The overtopping is caused by considering probable maximum flood (PMF) for the BRCH-J model input. The required data for implementing the BRCH-J model (listed in Table 1) are; fill material properties, the embankment geometry, cohesion, roughness factors, grain size, and the unit weight.

Result and Discussion

SWMM Calibration and Validation Process

A manual storm-by-storm SWMM calibration technique based on comparing the water bodies from two consecutive Sentinel-2A images has been implemented here. Based on Table 2, five rainfall events were used for the SWMM calibration process in which the best match value of the four parameters (impervious area percentage, SCS curve number, depth of storage in impervious and pervious areas) were recorded for each storm. Then, the mean value of the four recorded parameters was used to validate the model for the other five storms. Table 2 lists the total modeled runoff volumes and the associated observed storm events for the 10 rainfall scenarios. The modeled water volume in all precipitation events was identified by the mean value of these four parameters.

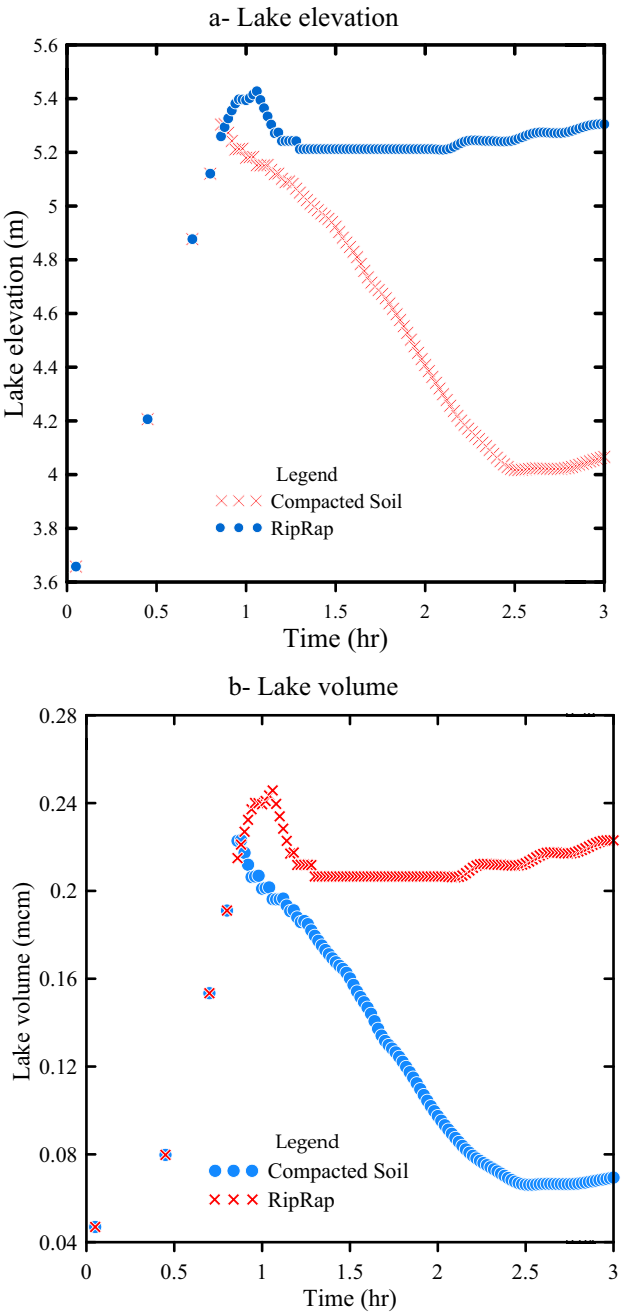

Fig. 6 The synthetic rainfall hyetographs via various methods **a** Chicago, **b** double triangular, and **c** instantaneous intensity (Chow) methods

Overall, the calibrated model underestimated observed water volumes for four rainfall events, while overestimating it for the other five rainfall scenarios, and when the rainfall height was less than 3 mm, the modeled and observed water volume were zero. In addition, only two of the storms exceeded 20% error, with storms 1 and 5 having the greatest errors, about 30 and 27%, respectively.

Table 1 The embankment properties

Embankment properties	Value
D50 (mm)	1.5
Porosity ratio	0.35
Unit weight (kg/m^3)	2249
Internal friction angle (°)	32
Cohesive strength (kg/m^2)	48.8
Ratio of D90 to D50	18
Roughness Strength	Strickler equation
Riprap size (mm)	250

Table 2 Runoff volumes in various rainfall scenarios

Rainfall event	Rainfall depth (mm)	Modeled/ calibration (m^3)	Observed (S2 images) (m^3)	Modeled/ validation (m^3)
1	5	281	198	–
2	3	0	0	–
3	3.5	169	204	–
4	68.5	29,103	36,430	–
5	128.5	114,995	83,950	–
6	9.5	–	735	858
7	57	–	29,684	24,571
8	101	–	98,566	111,400
9	4.5	–	238	197
10	83	–	47,864	54,705

Calibrated SWMM Evaluation

The Nash–Sutcliffe (NSE, defined by Gupta et al. 2009) and the ratio of root mean square error to the standard deviation of the observed series (RSR) were used for SWMM evaluation, as given by:

$$NSE = 1 - \frac{\sum_{t=1}^{n} \left(Q_{mo,t} - Q_{ob,t}\right)^2}{\sum_{t=1}^{n} \left(Q_{ob,t} - \mu_{ob}\right)^2} \tag{17}$$

$$RSR = \frac{\sqrt{\frac{\sum_{i=1}^{n} \left(Q_{mo,i} - Q_{ob,i}\right)^2}{n}}}{\sqrt{\sum_{i=1}^{n} \left(Q_{ob,i} - \mu_{ob}\right)^2}} \tag{18}$$

where n is the total number of time-steps, $Q_{ob,t}$ is the observed value at time step t, $Q_{mo,t}$ is the modeled value at time step t, and μ_{ob} is the mean of the observed values.

The goodness-of-fit for assessing the overall modelling performance based on the values of NSE and RSR was developed by Ritter and Munoz-Carpena (2013) and is tabulated in Table 3. Based on the observed and modeled water volumes data listed in Table 2, the NSE and RSR values were 0.913 and 0.093, respectively, confirming that the performance rating was very good and that an adequate number of storms had been used for SWMM calibration.

Triangular Fuzzy Number Representing the Load

The input data of the calibrated SWMM are 50 h duration storms, which are generated based on a single point of the local IDF in a 100-year return period and with three synthetic rainfall generation methods. The ratio of storm peak to storm duration in both Chicago and Chow (coefficient of the storm advancement), as well as the proportion of the length of the central triangular hyetograph to storm duration in the doubled triangular method, varies in each storm event. Besides, these uncertain coefficients are always between zero and one ($0 < r < 1$). Hence, with a 0.02 step increment, 150 synthetic rainfalls are generated (as shown in Fig. 7a, b, c). The mean and limit values of the calibrated SWMM outputs are then used to specify the definition parameters of the TFN representing the surface runoff, which is obtained as L = (0.0846, 0.17155, 0.14782), as depicted in Fig. 8. However, with 0.001 step increments of the uncertain parameter, a thousand storms are generated in each synthetic rainfall generation method, and it is observed that the definition parameters of the TFN representing the surface runoff stood approximately at the previous values.

Overall, it is observed that there is no direct relationship between the coefficient (r) and modeled runoff volume. Furthermore, the limit values of the SWMM output are obtained when the generated synthetic hyetographs are defined via the Chicago method, and the uncertain parameters are 0.98 and 0.9, respectively. In addition, when the double triangular method is implemented for generating synthetic storms, the modeled water volume is almost equal to 0.168 Mcm. It is mainly because, in this method, the peak intensity always occurs at the mid-time of the storm duration.

Triangular Fuzzy Number Representing the Resistance

A breach due to overtopping can occur at any water level above the crest elevation. Hence, the left endpoint of the TFN is the lake volume at the crest level was 0.167 mcm.

Table 3 The SWMM performance rating

Performance rating	Goodness-of-fit-test	
Very Good	NSE > 0.75	RSR < 0.5
Good	0.65 < NSE < 0.75	0.5 < RSR < 0.6
Satisfactory	0.5 < NSE < 0.65	0.6 < RSR < 0.7
Unsatisfactory	NSE < 0.5	RSR > 0.7

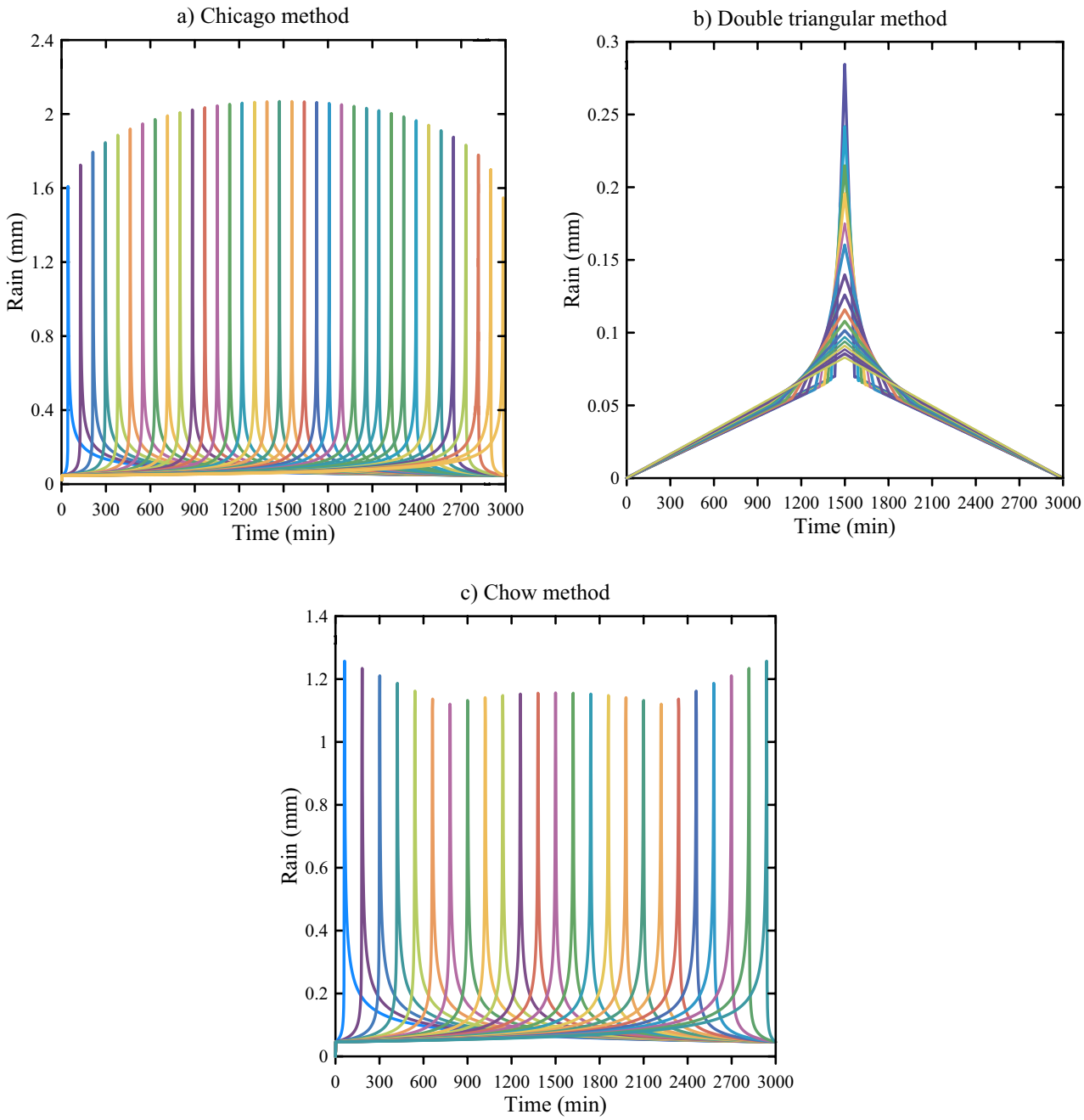

Fig. 7 The result of the Riprap protected and unprotected embankment breach simulation during PMF **a** lake water elevation, and **b** lake water volume

The BRCH-J model was used to simulate an embankment breach in two scenarios, without any rip-rap protection at the downstream face and with full rip-rap protection. Then the maximum water levels when the breach happened in these two scenarios were recorded at the vertex and the right end-point of the TFN, representing the lake capacity.

The maximum modeled water levels when the unprotected and rip-rap protected embankment breach began were at 0.335 m (about 1.1 ft.) and 0.426 m (about 1.4 ft.) above the crest elevation, corresponding to 0.223 and 0.245 Mcm lake water volume. So, the TFN representing the lake capacity (resistance) was obtained as R = (0.167, 0.223, 0.245) Mcm.

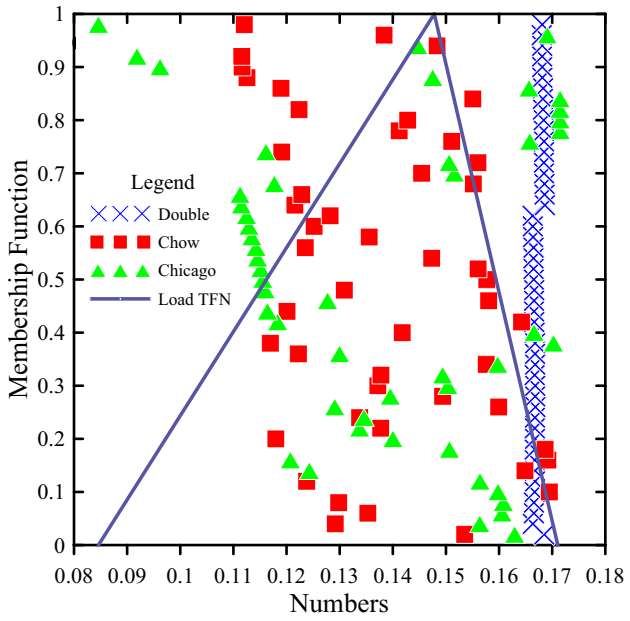

Fig. 8 The SWMM outputs based on three synthetic rainfall generation methods and the TFN representing the load based on the mean and the limit values of the SWMM outputs

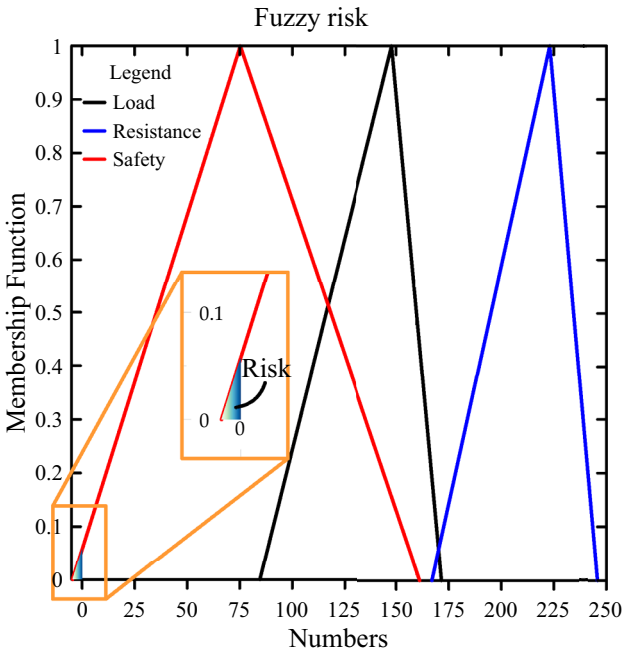

Fig. 9 The TFNs representing the load and the resistance and the safety margin of the embankment failure

Embankment Breach Fuzzy Risk Assessment

The fuzzy risk was calculated using the difference between two TFN quantities representing the resistance and load (as the ratio of the integral of the negative portion of their difference to the entire area of their difference). The TFNs representing the load and resistance, together with the fuzzy safety margin, are shown in Fig. 9. Note that when the left endpoint of the TFN representing the resistance (R1 in Eq. 8) exceeds the right endpoint of the TFN representing the load (L_3 in Eq. 8), the risk value is zero. The converse holds when the right endpoint of the TFN representing the resistance (R_3) is less than the left endpoint (L_1) of the TFN representing the load.

Finally, based on Eq. 8, and knowing that L = (0.0846, 0.17155, 0.14782) Mcm, the fuzzy risk of an embankment breach is 0.15%. Since the standard design storm for the lake and embankment system is 100 year recurrence intervals (which means an accepted failure risk of 1%), the available lake storage volume exceeds the expected capacity, and the risk of embankment breach due to overtopping is relatively low. However, the result indicates that the risk of failure is increased dramatically by decreasing the embankment height and reaches its maximum value (100% risk) if the embankment height is reduced to 4 m.

Based on the initial design standard, the hydrological return period of the existing Golgohar drainage system is 100 years (again, a 1% accepted risk). The fuzzy theory was used to reassess the risk of the mine site's drainage system. So, the SWMM (rainfall-runoff model) software and a breach erosion model were analyzed to obtain the TFN. Then, on the basis that both TFNs must match, the fuzzy risk is the difference between their quantities (the integral of the negative portion to the entire area of their difference). Hence, the fuzzy risk obtained was 0.15%, indicating that the available stormwater storage capacity was adequate. In other words, based on the load and resistance theory, the hydrological return period concept, and the fuzzy approach, we can conclude that the available storage volume of the lake is satisfactory. Thus, using remote sensing and the fuzzy theory provides a tool to evaluate a mine site's safety, which was not possible using the traditional (probabilistic) method.

Summary and Conclusion

As many mine sites are located in remote areas with poor records of hydrological data, implementing the classical probability approaches for flood risk assessment are very unreliable. A fuzzy arithmetic risk assessment method based on the alpha-cut principle was used to evaluate the risk of embankment failure within a lake drainage system at the Golgohar mine site. The definition parameters of the two TFNs were obtained directly from a calibrated SWMM and a breach erosion model (BRCH-J). Since the Sentinel-2A revisit time is 10 days, tuning the SWMM with a series of two consecutive S2 images is a useful technique, especially when there is no hydrometric station

(runoff data) available in the catchment. Three synthetic hyetograph generation methods (Chicago method, double triangular, and instantaneous intensity) based on a single point of the local IDF curve were implemented as inputs for the SWMM model. The mean and limit values of the SWMM outputs were used to define the TFN representing the load, obtained as L = (0.0846, 0.17155, 0.14782) Mcm. Since the embankment breach due to overtopping can occur at any water level above the crest level, and only some parts of its downstream face are riprap-protected, the breach processes can initiate at three levels. Hence, the lake volumes at three stages (at the crest level, once the unprotected and riprap-protected embankment breach happens) were recorded. The TFN representing the lake capacity (resistance) was calculated as R = (0.167, 0.223, 0.245) Mcm. As a result, the fuzzy risk of the embankment breach for 100-year recurrence intervals was obtained as 0.15%. Since the value of the accepted risk for the storage system is 1% (based on the initial design standard), the available stormwater storage volume exceeds the expected capacity, and the risk of an embankment failure is relatively low. Although this paper's methodology only focused on a mine site, the proposed fuzzy approach could be useful for any remote area. Overall, this approach can be relied on as a way to evaluate the risk of an entire drainage system when the historical data is scarce.

This paper describes a new method to tackle the risk of failure in a mine site drainage system, using only a mere number of Sentinel images. As many mine sites are located in remote areas with a poor historical record, using remote sensing techniques can provide mining engineers with additional insight. The state-of-the-art rainfall-runoff model calibration methodology described here can be used as a guideline for the proper design of post-mining drainage systems that reflect rehabilitation success and will lead to the establishment of a sustainable native ecosystem. The fuzzy methodology should be used for risk assessment at areas where the traditional (probabilistic) method is not helpful, such as at remote mine sites. Given our findings, remote sensing can be used to calibrate the rainfall-runoff relationship to design a new drainage system or assess the risk of failure of an existing surface water storage and conveyance system.

The TFN was used here, due to its simplicity for handling fuzzy operations, to represent the uncertainties related to load and resistance. Investigating the other types of fuzzy numbers, such as trapezoidal and Gaussian membership functions, remains work for future investigation. Moreover, the alpha-cut principle was used for a breach fuzzy risk assessment. Fuzzy arithmetic based on approximation methods (e.g. arithmetic operation with the L-R type) for computing the fuzzy risk products is an alternative method of the alpha-cut principle. This approach has not been pursued here and needs more investigation. This paper's technique only focused on a remote mine site. Investigating the results of this research on other basins with poor historical records is highly recommended and is left for further studies. Also, the synthetic rainfall generation with a single point of the IDF curves does not represent the actual historical rainfall duration. Given this, generating rainfall scenarios based on other methods is of particular interest. However, this approach has not been pursued here and is left for future work.

Acknowledgements The authors thank the anonymous reviewers for their detailed and valuable comments and suggestions.

Data Availability All data, models, and code generated or used during the study appear in the submitted article. The available data is listed in Table 1.

References

Barco J, Wong KM, Stenstrom MK (2008) Automatic calibration of the US EPA SWMM model for a large urban catchment. J Hydraul Eng 134(4):466–474. https://doi.org/10.1061/(ASCE)0733-9429(2008)134:4(466)

Behrouz MS, Zhu Z, Matott LS, Rabideau AJ (2020) A new tool for automatic calibration of the Storm Water Management Model (SWMM). J Hydrol 581:124436. https://doi.org/10.1016/j.jhydrol.2019.124436

Caradot N, Granger D, Chapgier J, Cherqui F, Chocat B (2011) Urban flood risk assessment using sewer flooding databases. Water Sci Technol 64(4):832–840. https://doi.org/10.2166/wst.2011.611

Chaira T (2019) Fuzzy set and its extension. Wiley Online Library

Cheng WM, Huang CL, Hsu NS, Wei CC (2017) Risk analysis of reservoir operations considering short-term flood control and long-term water supply: a case study for the Da-Han Creek Basin in Taiwan. Water J 9(6):424. https://doi.org/10.3390/w9060424

Chow VT, Maidment D, Mays LW (1988) Applied Hydrology. McGraw-Hill

Dent S, Hanna RB, Wright LT (2004) Automated calibration using optimization techniques with SWMM RUNOFF. J Water Manag Model 32:45–52. https://doi.org/10.14796/JWMM.R220-18

Flatley A, Markham A (2021) Establishing effective mine closure criteria for river diversion channels. J Environ Manage 287:112287. https://doi.org/10.1016/j.jenvman.2021.112287

Fu X, Tao T, Wang H, Hu T (2013) Risk assessment of lake flooding considering propagation of uncertainty from rainfall. J Hydrol Eng 18(8):1041–1047. https://doi.org/10.1061/(ASCE)HE1943-5584.0000700

Gupta HV, Kling H, Yilmaz KK, Martinez GF (2009) Decomposition of the mean squared error and NSE performance criteria: implications for improving hydrological modelling. J Hydrol 377(1–2):80–91. https://doi.org/10.1016/J.JHYDROL.2009.08.003

Hartman HL, Mutmansky JM (2002) Introductory mining engineering. John Wiley & Sons

ISO (2009) Risk management: principles and guidelines. International Standards Organization, Geneva, p 24

Jahanshahi R, Zare M (2017) Delineating the origin of groundwater in the Golgohar mine area of Iran using stable isotopes of 2H and 18O and hydrochemistry. Mine Water Environ 36(4):550–563. https://doi.org/10.1007/s10230-017-0444-6

Keifer CJ, Chu HH (1957) Synthetic storm pattern for drainage design. J Hydraul Eng 83(4):1332. https://doi.org/10.1061/JYCEAJ.0000104

Lee KT, Ho JY (2008) Design hyetograph for typhoon rainstorms in Taiwan. J Hydrol Eng 13(7):647–651. https://doi.org/10.1061/(ASCE)1084-0699(2008)13:7(647)

Lee EH, Kim JH (2019) Development of a reliability index considering flood damage for urban drainage systems. KSCE J Civ Eng 23(4):1872–1880. https://doi.org/10.1007/s12205-019-0408-4

Mancipe-Munoz NA, Buchberger SG, Suidan MT, Lu T (2014) Calibration of rainfall-runoff model in urban watersheds for stormwater management assessment. J Water Resour Plan Manag 140(6):05014001. https://doi.org/10.1061/(ASCE)WR.1943-5452.0000382

Manero A, Kragt M, Standish R, Miller B, Jasper D, Boggs G, Young R (2020) A framework for developing completion criteria for mine closure and rehabilitation. J Environ Manage 273:111078. https://doi.org/10.1016/j.jenvman.2020.111078

Maus V, Giljum S, Gutschlhofer J, da Silva DM, Probst M, Gass SL, Luckeneder S, Lieber M, McCallum I (2020) A global-scale data set of mining areas. Sci 7(1):1–13. https://doi.org/10.6084/m9.figshare.12594248

Rezazadeh Baghal S, Khodashenas SR (2022a) Fuzzy number linear programming technique for design of rectangular canals. J Irrig Drain Eng 148(8):04022027. https://doi.org/10.1061/(ASCE)IR.1943-4774.00001685

Rezazadeh Baghal S, Khodashenas SR (2022b) Risk assessment of storm sewers in urban areas using fuzzy technique and monte carlo simulation. J Irrig Drain Eng 148(8):04022028. https://doi.org/10.1061/(ASCE)IR.1943-4774.0001696

Ritter A, Munoz-Carpena R (2013) Performance evaluation of hydrological models: statistical significance for reducing subjectivity in goodness-of-fit assessments. J Hydrol 480:33–45. https://doi.org/10.1016/j.jhydrol.2012.12.004

Rossman LA (2010) Storm water management model user, s manual version 5.0. National Risk Management Research Laboratory

Salah A, Moselhi O (2015) Contingency modelling for construction projects using fuzzy-set theory. Eng Constr Archit Manag 22(2):214–241. https://doi.org/10.1108/ECAM-03-2014-0039

Salas JD, Heo JH, Lee DJ, Burlando P (2013) Quantifying the uncertainty of return period and risk in hydrologic design. J Hydrol Eng 18(5):518–526. https://doi.org/10.1061/(ASCE)HE.1943-5584.0000613

Sangal S, Bonema SR (1994) A methodology for calibrating SWMM models. J Water Manag Model. https://doi.org/10.14796/JWMM.RI76-24

Shahba S, Arjmandi R, Monavari M, Ghodusi J (2017) Application of multi-attribute decision-making methods in SWOT analysis of mine waste management (case study: Sirjan's Golgohar iron mine, Iran). Resour 51:67–76. https://doi.org/10.1016/j.resourpol.2016.11.002

Shamsi UMS, Koran J (2017) Continuous calibration. J Water Manag Model 25:1–9. https://doi.org/10.14796/JWMM.C414

Shrestha B, Reddy R, Duckstein L (1990) Fuzzy reliability in hydraulics. Proceedings 1st International Symposium on Uncertainty Modeling and Analysis. IEEE, College Park, pp 167–172

Singh V (1996) Dam breach modeling technology. Springer Science & Business Media

Su H, Wen Z (2013) Interval risk analysis for gravity dam instability. Eng Fail Anal 33:83–96. https://doi.org/10.1016/j.engfailanal.2013.04.027

Sun S, Fu G, Djordjević S, Khu ST (2012) Separating aleatory and epistemic uncertainties: probabilistic sewer flooding evaluation using probability box. J Hydrol 420:360–372. https://doi.org/10.1016/j.jhydrol.2011.12.027

Ursino N (2015) Risk analysis of sustainable urban drainage and irrigation. Adv Water Resour 83:277–284. https://doi.org/10.1016/j.advwatres.2015.06.011

Worldwide (2010) Guidebook for evaluating mining project EIAs. Environmental Law Alliance Worldwide, Eugene

Yang X, Zhao S, Qin X, Zhao N, Liang L (2017) Mapping of urban surface water bodies from Sentinel-2 MSI imagery at 10 m resolution via NDWI-based image sharpening. Remote Sens 9(6):596. https://doi.org/10.3390/rs9060596

Zadeh LA (1973) Outline of a new approach to the analysis of complex systems and decision processes. IEEE Trans Syst Man Cybern 3(1):28–44. https://doi.org/10.1109/TSMC.1973.5408575

Zha Y, Gao J, Ni S (2003) Use of normalized difference built-up index in automatically mapping urban areas from TM imagery. Int J Remote Sens 24(3):583–594. https://doi.org/10.1080/01431160304987